oxychlor on elution from the primary column. Results are presented on Table V together with the limit of detection (LOD) for each pesticide present in a 1.5-L groundwater sample. When gradient elution reversed-phase HPLC is operated in the low-wavelength region (220–230 nm), more than the amplitude of the electrical noise is the slope of the base-line drift, which depends on the content of UV-absorbing impurities present in the mobile phase, which defines the LOD of the analysis. Under the chromatographic conditions selected, the LODs of this method were estimated by assuming arbitrarily that 0.5 cm was the minimum peak height that could be used with reasonable confidence. The LODs for base–neutral pesticides were estimated from peaks produced by them on the cyano column. LODs reported in the table refer to extraction of 1.5 L of a groundwater sample. Thus, the LODs for river waters have to be increased by a factor 3 and for drinking water decreased by a factor 0.75, as this method involves extraction of 0.5 and 2 L of river and drinking waters, respectively.

Registry No. DDT, 50-29-3; 2,4-D, 94-75-7; MCPA, 94-74-6; 2,4,5-T, 93-76-5; 2,4-DB, 94-82-6; MCPB, 94-81-5; 2,4,5-TP, 93-72-1; H_2O, 7732-18-5; oxamyl, 23135-22-0; methomyl, 16752-77-5; mevinphos I, 7786-34-7; chloridazon, 1698-60-8; dimethoate, 60-51-5; hexazinone, 51235-04-2; aldicarb, 116-06-3; metoxuron, 19937-59-8; simazine, 122-34-9; bromacil, 314-40-9; monuron, 150-68-5; cyanazine, 21725-46-2; metribuzin, 21087-64-9; dichlorvos, 62-73-7; propoxur, 114-26-1; carbofuran, 1563-66-2; pirimicarb, 23103-98-2; atrazine, 1912-24-9; chlortoluron, 15545-48-9; fluometuron, 2164-17-2; carbaryl, 63-25-2; diazinon, 333-41-5; isoproturon, 34123-59-6; ethiofencarb, 29973-13-5; monolinuron, 1746-81-2; diuron, 330-54-1; difenoxuron, 14214-32-5; metobromuron, 3060-89-7; paraoxon, 311-45-5; propachlor, 1918-16-7; propham, 122-42-9; propazine, 139-40-2; propanil, 709-98-8; terbutylazine, 5915-41-3; dichlobenil, 1194-65-6; linuron, 330-55-2; azinphos-methyl, 86-50-0; chloroxuron, 1982-47-4; fenamiphos, 22224-92-6; chlorbromuron, 13360-45-7; molinate, 2212-67-1; propyzamide, 23950-58-5; parathion-methyl, 298-00-0; chlorpropham, 101-21-3; metolachlor, 51218-45-2; procymidone, 32809-16-8; malathion, 121-75-5; fenitrothion, 122-14-5; rotenone, 83-79-4; azinphos-ethyl, 2642-71-9; neburon, 555-37-3; eptam, 759-94-4; fenthion, 55-38-9; parathion-ethyl, 56-38-2; sulfallate, 95-06-7; coumaphos, 56-72-4; cycloate, 1134-23-2; phorate, 298-02-2; phoxim, 14816-18-3; disulfoton, 298-04-4; pirimiphos-methyl, 29232-93-7; butylate, 2008-41-5; methoxychlor, 72-43-5; chlorpyriphos, 2921-88-2; pendimethalin, 40487-42-1; pirimiphos-ethyl, 23505-41-1; trifluralin, 1582-09-8; bromophos-ethyl, 4824-78-6; fenvalerate, 51630-58-1; bentazone, 25057-89-0; dicamba, 1918-00-9; bromoxymil, 1689-84-5; dinitro-*o*-cresol, 534-52-1; coumafuryl, 117-52-2; ioxynil, 1689-83-4; dichloroprop, 120-36-5; mecoprop, 7085-19-0; warfarin, 81-81-2; dinoseb, 88-85-7; dinoterb, 1420-07-1; pentachlorophenol, 87-86-5.

Literature Cited

(1) Di Corcia, A.; Carfagnini, G.; Marchetti, M. *Ann. Chim.* **1987**, *77*, 825–835.
(2) Di Corcia, A.; Marchetti, M.; Samperi, R. *J. Chromatogr.* **1987**, *405*, 357–363.
(3) Battista, M.; Di Corcia, A.; Marchetti, M. *Anal. Chem.* **1989**, *61*, 935–939.
(4) Di Corcia, A.; Marchetti, M.; Samperi, R. *Anal. Chem.* **1989**, *61*, 1363–1367.
(5) Di Corcia, A.; Marchetti, M. *J. Chromatogr.* **1991**, *541*, 365–373.
(6) Di Corcia, A.; Samperi, R. *Anal. Chem.* **1990**, *62*, 1490–1494.
(7) Borra, C.; Di Corcia, A.; Marchetti, M.; Samperi, R. *Anal. Chem.* **1986**, *58*, 2048–2052.
(8) Di Corcia, A.; Marchetti, M. *Anal. Chem.* **1991**, *63*, 580–585.
(9) Andreolini, F.; Borra, C.; Caccamo, F.; Di Corcia, A.; Samperi, R. *Anal. Chem.* **1987**, *59*, 1720–1725.
(10) Saleh, F. H.; Ong, W. A.; Chang, D. Y. *Anal. Chem.* **1989**, *61*, 2792–2800.
(11) Di Corcia, A.; Marchetti, M.; Marcomini, A.; Samperi, R. *Anal. Chem.* **1991**, *63*, 1179–1182.
(12) Munch, D. J.; Graves, R. L.; Maxey, R. A.; Engel, T. M. *Environ. Sci. Technol.* **1990**, *24*, 1446–1451.

Received for review April 29, 1991. Revised manuscript received June 26, 1991. Accepted July 1, 1991.

Synthesis of Peroxyacetyl Nitrate in Air by Acetone Photolysis

Peter Warneck* and Thomas Zerbach

Max-Planck-Institut für Chemie (Otto-Hahn-Institut), D 6500 Mainz, Germany

■ The photodecomposition of acetone in air with NO_2 admixed has been used to generate peroxyacetyl nitrate (PAN) either by batch synthesis in an isolated flask or in a continuous-flow reactor. With NO_2 mixing ratios near 10 ppm, the method converts in the first case 88% of NO_2 to PAN and ~6% to methyl nitrate within a time period of a few minutes. In the second case, the conversion is ~90% and 10%, respectively. The reproducibility is better than 5%. The PAN mixing ratio produced by batch synthesis declines exponentially with time due to wall-catalyzed thermal decomposition.

Introduction

Peroxyacetyl nitrate (PAN) is an important nitrogen compound in the atmosphere. It originates from the addition of oxygen and nitrogen dioxide to acetyl radicals, which are generated in precursor reactions involving carbonyl compounds such as acetaldehyde and acetone (*1*). As a product of photochemical air pollution, PAN has been suggested to serve as an indicator for photochemical smog (*2, 3*). Under these conditions it is one of the compounds causing eye irritation and plant damage (*4, 5*). As a natural constituent of the background troposphere, PAN provides a reservoir of loosely bound NO_2, because NO_2 is released when PAN undergoes thermal decomposition at favorably high temperatures (*6*). In addition, thermal decomposition is a source of acetylperoxy radicals, which react further to produce methylperoxy, hydroperoxy, and ultimately hydroxyl radicals by reactions with NO and oxygen. Singh (*1*), in a recent review of reactive nitrogen, has furnished a summary of the occurrence and the effects of PAN in the troposphere.

The currently preferred method for the determination of PAN in air is gas chromatography in combination with the electron capture detector (ECD). Its sensitivity is excellent but subject to some variability, so that frequent calibrations are needed. In view of the thermal instability of PAN, some effort is required to make available, for the purpose of calibration, a PAN/air mixture with known mixing ratio. A widely used method is to synthesize PAN in an inert solvent such as octane, stabilize it by refrigeration, and then prepare from it PAN/air mixtures by on-site dilution with air (*7–10*). Alternatively, PAN may

 0013-936X/92/0926-0074$03.00/0

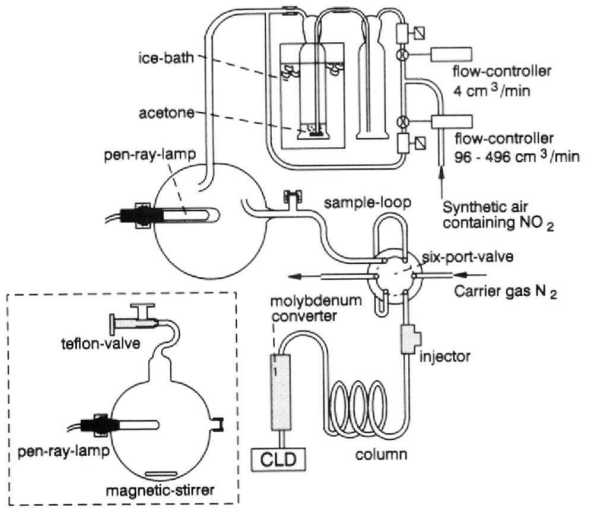

Figure 1. Experimental setup for the continuous generation of PAN. Inset: Isolated flask for batch synthesis.

also be generated photochemically, either in a closed flask or in a flow system, provided the photochemical process yields acetyl radicals (*10–12*). In particular, Meyrahn et al. (*10*) have explored the utility of acetone photodecomposition for this purpose and reported an excellent reproducibility of PAN mixing ratios in individual runs. This method is based on the reaction sequence

$$CH_3COCH_3 + h\nu \rightarrow CH_3CO + CH_3 \quad (1)$$

$$CH_3CO + O_2 \rightarrow CH_3COO_2 \quad (2)$$

$$CH_3COO_2 + NO_2 \rightarrow CH_3COO_2NO_2 \quad (PAN) \quad (3)$$

Under suitable conditions almost the entire supply of NO_2 can be converted to PAN within a relatively short period of time. However, when such PAN/air mixtures are produced in a closed flask, the PAN concentration subsequently decreases with time due to thermal decomposition so that the method requires corrections. We have now studied this behavior in more detail and report our results below. In addition, we describe a simple flow technique for the continuous generation of PAN based on the same chemical system.

Experimental Section

Acetone was photolyzed by means of a Penray mercury lamp inserted in a 1-L glass flask as shown in Figure 1. A Teflon-coated silicone rubber septum was attached to the flask for the injection of acetone and the withdrawal of samples with appropriate syringes. A magnetic stirrer was provided to achieve a homogeneous gas mixture. The batch synthesis of PAN was similar to the procedure described previously (*10*). The flask was evacuated with a rotary pump, filled with artificial air containing ~10 ppm NO_2, and isolated with a Teflon-stoppered valve. About 10 μL of liquid acetone were then injected under stirring, and the mixture was irradiated for 5 min. The continuous generation of PAN was also carried out with artificial air containing ~10 ppm NO_2 as shown in Figure 1. In this case, a fraction of the gas flow (0.8–4%) was diverted to pass through an ice-cooled bubbler filled with acetone, and this part of the airflow was subsequently reunited with the main airflow before it entered the flask.

The emission from the mercury lamp is concentrated in the 254-nm Hg resonance line. The total photon flux emitted was determined in a separate experiment by means of ferric oxalate actinometry (*13*). As described elsewhere (*14*), the lamp was placed along the axis of a cylindrical quartz vessel containing an aqueous solution of 10 mmol/L $K_3Fe(C_2O_4)_3$ in 0.1 N sulfuric acid. The amount of iron(II) generated after 15–30 s of irradiation (quantum yield 1.25) was determined by optical absorption of the iron–1,10-phenanthroline complex [$\epsilon = 1.1 \times 10^4$ L/(mol cm) at 510 nm wavelength]. A total photon flux of 3.2×10^{17} photons/s was calculated.

PAN and methyl nitrate ($MeONO_2$) were determined by gas chromatography using an NO chemiluminescence detector (CLD). The column consisted of a 25 cm × 2 mm i.d. helical glass tube packed with 10% Carbowax 600 on Chromosorb HP (80/100 mesh). The column was kept fairly short in order to minimize losses of PAN on the column. Under isothermal conditions at room temperature (22 °C), a nitrogen carrier gas flow of 24 cm^3/min resulted in retention time of 0.86 min for $MeONO_2$ and 2.76 min for PAN when the sample was introduced via a 4-cm^3 sample loop. Smaller sample volumes were injected directly into the carrier gas stream with a gas-tight syringe. Behind the column the gases flowed through a 5 cm × 2 mm i.d. stainless steel tube filled with molybdenum chips. The tube was heated to 370 °C, whereby PAN and methyl nitrate were quantitatively reduced to NO. The gases then entered a reaction chamber where they were mixed with oxygen, which was partly ozonized by means of a silent discharge. The chemiluminescence resulting from the reaction of NO with O_3 was registered with a photomultiplier; the signal pulses were amplified and processed with a pulse counter/rate meter. An integrating recorder was used for peak area determination. The instrument was calibrated with a mixture of 1.6 ppm NO in nitrogen. Schurath et al. (*15*) have determined on-column losses of PAN as a function of contact time and temperature (20 and 30 °C). From their data we estimate that for our conditions (PAN retention time 2.75 min and $T = 22$ °C) the amount of PAN leaving the column and entering the detector is 82% of the amount injected. An appropriate correction was applied.

Results

Batch Synthesis. As noted previously (*10*), the irradiation of a mixture of acetone and NO_2 in air converted almost the entire amount of NO_2 present to PAN within a 4–5-min time interval. Mixing ratios of PAN thus obtained were well reproducible provided the vessel was preconditioned; that is, more than one photolysis run was carried out in the same vessel. In all experiments the mixing ratios of PAN and $MeONO_2$ rose fairly linearly until they reached a plateau whereupon the conversion of NO_2 was complete. Further tests showed that the final mixing ratios were independent of total pressure in the range (1.0–1.3) × 10^5 Pa and of the applied volume of acetone in the range 2–15 μL, but they were essentially proportional to the initial mixing ratio of NO_2. Table I shows the reproducibility that can be achieved under various conditions. About 94% of the initial NO_2 is recovered in the form of PAN and methyl nitrate, with a contribution of the latter amounting to ~7% of the observed product yield.

A major point of interest was the stability of such PAN/air mixtures. In order to investigate the behavior of PAN and $MeONO_2$ a mixture was prepared as describe above, the flask was thermostated, and its contents were analyzed for periods lasting up to 8 h. Figure 2 shows that the PAN mixing ratio decreased with time, whereas that of $MeONO_2$ stayed constant. The PAN decay was always exponential, following a first-order rate law with $m = m_0 \exp(-kt)$, where k is a rate constant and t is time. Rate

Table I. Mixing and Product Ratios for PAN and $MeONO_2$ Generated by the Batch Procedure under Various Initial Conditions[a]

			mixing ratio, ppm		product ratio	
10^5p, Pa	NO_2,[b] ppm	acetone vol, μL	PAN	$MeONO_2$	Σ(products)/NO_2	$MeONO_2$/PAN
1.09 ± 0.05	14	2–15	11.86 ± 0.60	0.89 ± 0.10	0.91 ± 0.05	0.076 ± 0.006
1.03–1.13	14	10	12.25 ± 0.73	0.84 ± 0.08	0.94 ± 0.06	0.071 ± 0.004
1.12 ± 0.02	10.4	10	9.11 ± 0.46	0.71 ± 0.13	0.94 ± 0.06	0.073 ± 0.010
1.13 ± 0.02	7.7	10	6.53 ± 0.25	0.64 ± 0.07	0.93 ± 0.04	0.097 ± 0.007

[a] Irradiation time 5 min, T = 22 °C; averages of five runs each. [b] Initial NO_2.

Table II. PAN Decay Rate Coefficients in the Same Flask for Various Temperatures

temp, K	$[NO_2]_0$, ppm	$[PAN]_0$, ppm	$[MeONO_2]_0$, ppm	10^5k, s^{-1}	n[a]
278	14	12.4 ± 0.9	0.86 ± 0.08	2.96 ± 0.80	1 (23)
285	14	13.2 ± 0.9	0.71 ± 0.05	3.45 ± 0.74	1 (27)
295	14	12.3 ± 0.7	0.88 ± 0.04	8.02 ± 0.65	5 (154)
298	14	12.2 ± 0.7	0.80 ± 0.11	8.70 ± 1.63	5 (15)
304	10.6	9.0 ± 0.4	0.73 ± 0.13	20.60 ± 1.80	5 (73)
318	14	12.7 ± 1.9	0.82 ± 0.25	43.60 ± 2.50	1 (16)

[a] Number of runs; values in parentheses, number of data points.

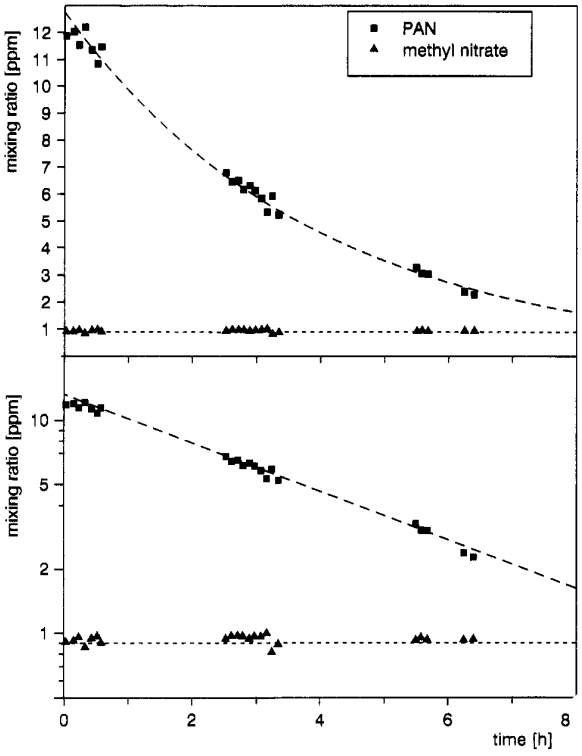

Figure 2. Decrease of PAN mixing ratio with time after synthesis (m_{NO_2} = 14 ppm): (a, top) linear scale; (b, bottom) semilogarithmic scale. The mixing ratio of methyl nitrate is shown for comparison.

coefficients were determined as a function of temperature by performing linear regression analyses of the data in a semilogarithmic representation similar to that shown in Figure 2b. The results are compiled in Table II. The temperature dependence of the rate constant is in harmony with the usual Arrhenius expression $k = k_0 \exp(-E_A/RT)$, where E_A is the activation energy, R = 3.814 J/(mol K) is the gas constant, and T is the absolute temperature. A value of E_A = 62.7 ± 8.4 kJ/mol was calculated from the data in Table II. The value is considerable smaller than the activation energies found by several other investigators (*16–18*) for the dissociation process

$$PAN \rightarrow CH_3COO_2 + NO_2$$

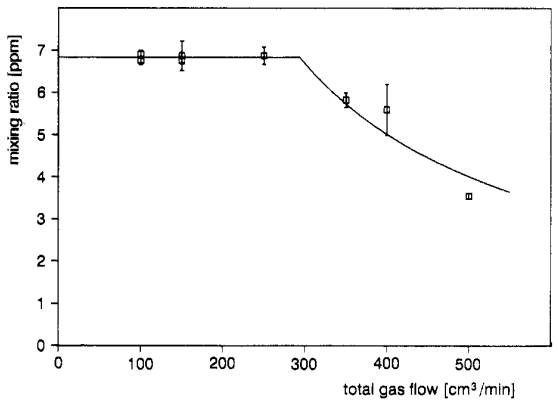

Figure 3. Output of PAN from the continuous-flow reactor as a function of the total volume flow rate (m_{NO_2} = 7.7 ppm). The solid line was calculated as described in the text.

in the gas phase. Their values fell into the range 104–112 kJ/mol. It appears, therefore, that the decomposition of PAN under the present conditions is mainly catalyzed by wall reactions. Indeed, use of a different flask with nearly the same volume instead of the flask leading to the above results, but keeping the other experimental conditions the same, caused a marked change (~50%) in the rate constant obtained.

Continuous-Flow Method. The limited stability of PAN/air mixtures prepared by batch synthesis led us to explore a flow method based on the experimental arrangement shown in Figure 1 in the hope of generating a continuous flow of PAN with constant mixing ratio. In this case, acetone was added to the airflow by saturating a portion of it from a supply of liquid acetone kept in an ice bath. This was a simple procedure to keep the saturation vapor pressure both constant and at a level low enough to prevent condensation in the flow tube. We expected the PAN mixing ratio to depend on the total flow rate, u_{tot}, since it determined the residence time τ of the gases in the photolytic reactor. This dependence was indeed observed. Figure 3 shows the PAN mixing ratio in the airstream emerging from the reaction vessel as a function of the total flow rate. The NO_2 content in the air supply used in these experiments was 7.7 ppm by volume.

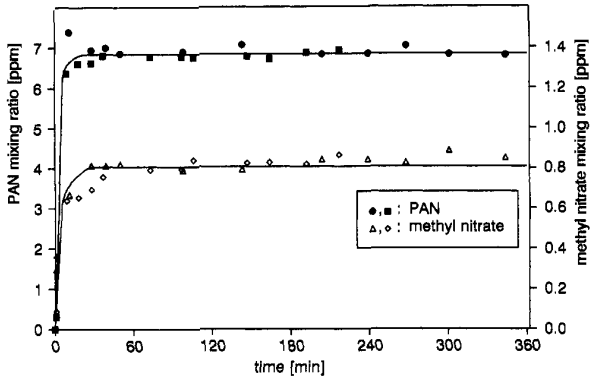

Figure 4. Output of PAN and methyl nitrate from the continuous-flow reactor; stability with time for two independent runs indicated by different symbols.

Under optically thin conditions, which apply here, the PAN mixing ratio in the air leaving the reactor is given by

$$m_{PAN} = (\phi\sigma m_{ac} dI_o/V)\tau$$

or

$$m_{PAN} = (\phi\sigma m_{ac} dI_o/u_{tot}) \qquad \text{with } \tau = V/u_{tot}$$

Here, $\phi = 0.76$ is the quantum yield for acetone photodecomposition at 254 nm, $\sigma = 2.5 \times 10^{-20}$ cm^2/molecule is the absorption cross section at this wavelength, $I_o = 3.2 \times 10^{17}$ photons/s is the photon flux, $d \approx 6$ cm is the optical path length, and $V = 1135$ cm^3 is the volume of the reactor. Values for the quantum yield and the absorption cross section were taken from Meyrahn et al. (*19*). From the above formulas the PAN mixing ratio is seen to rise with increasing acetone mixing ratio m_{ac} and τ (or decreasing u_{tot}), and this relation should hold until the supply of NO_2 is exhausted. Then, m_{PAN} would become constant. In the flow arrangement chosen here, the acetone mixing ratio was a function of the total flow rate, because the flow u_s through the acetone saturator was kept constant at 0.07 cm^3/s while the total flow rate was varied. Accordingly

$$m_{ac} = (p_{ac}/p_{air})(u_s/u_{tot})$$

so that the PAN mixing ratio should depend on the reciprocal of u_{tot}^2. Figure 3 includes, for comparison with the experimental data, PAN yields calculated on the basis of the above formulas. With a saturation vapor pressure of $p_{ac} = 88$ hPa at 0 °C (*20*), the acetone mixing ratio was calculated to range from 700 to 3500 ppm, which was very similar to the mixing ratios employed in the batch preparation of PAN.

Finally, it was important to establish the reproducibility of continuous PAN generation. Figure 4 shows the behavior of PAN mixing ratios produced continuously over a period of 6 h under experimentally constant conditions. Stationary values were reached after 15–20 min; thereafter the PAN mixing ratio stayed essentially constant. As for the batch synthesis procedure, it was found that for an almost complete conversion of NO_2 to PAN, that is for flow rates of 290 cm^3/min or less, the PAN/air mixtures obtained were very reproducible from experiment to experiment.

Table III shows averages for the mixing ratios of PAN and $MeONO_2$ obtained from time series measurements on the one hand, and independent runs on separate days on the other hand. In the first case, the averages and standard deviations indicate the reproducibility for the time intervals given. The second case combines the individual data to demonstrate the overall precision and repeatability of PAN mixing ratios produced by continuous generation.

Table III. Reproducibility and Repeatability of Results for the Continuous-Flow Method

gas flow rate, cm^3/min	time interval, min	no. of data points	mixing ratio, ppm PAN	mixing ratio, ppm $MeONO_2$
100	199	10	6.76 ± 0.09	0.80 ± 0.05
100	316	10	6.91 ± 0.09	0.83 ± 0.03
150	328	11	6.76 ± 0.08	0.75 ± 0.01
150	264	10	6.88 ± 0.35	0.67 ± 0.13
250	169	8	6.88 ± 0.21	0.74 ± 0.03
350	218	9	5.82 ± 0.17	0.48 ± 0.06
400	201	10	5.59 ± 0.60	0.57 ± 0.09
500	153	6	3.55 ± 0.06	0.63 ± 0.01
100–250	169–328	49	6.87 ± 0.27[a]	0.75 ± 0.11[a]
100–250	169–328	5	6.84 ± 0.06[b]	0.76 ± 0.05[b]

[a] Average of all data points. [b] Average of the averages for the first five runs.

Discussion

The present results confirm the utility of acetone photolysis in the generation of PAN in air. The reproducibility for batch synthesis is ~5%, that for continuous-flow generation is 3%. In both cases, the precision is probably determined largely by our analytical technique rather than by the duplication of PAN results. Batch synthesis is rapid, but the PAN/air mixture obtained has a limited stability and the concentration of PAN declines with time. The decay constant at 25 °C is 1 order of magnitude greater than that reported by us previously (*10*) for wall-conditioned flasks, when we had synthesized PAN by the reaction of nitric acid with peroxyacetic acid according to the procedure of Nielsen et al. (*7*). In that case we had also found that the decomposition of PAN was wall-catalyzed.

Under the present conditions it is likely that acetone photooxidation products such as formaldehyde are responsible for the enhanced PAN decay. In a few trial runs, we found that the injection of 5 μL of a 30% aqueous solution of formaldehyde into the flask accelerated the PAN decay, whereas the injection of a similar amount of acetaldehyde slowed it down. Kirchner (*21*) reported a similar decay effect following the addition of propanol to gas mixtures containing PAN, which caused an equivalent production of peroxypropionyl nitrate (PPN). In other experiments (*22*) we have found that PPN is quantitatively converted to PAN after the addition of excess acetaldehyde to the gas mixture. These observations may be rationalized by reactions of peroxyacyl radicals, generated from the thermal decomposition of the peroxyacyl nitrates, with the aldehydes. If peroxyacyl radicals abstract the aldehydic hydrogen atom, for example

$$CH_3CH_2COO_2 + CH_3CHO \rightarrow CH_3CH_2COO_2H + CH_3CO \quad (4)$$

the new acyl radical can then add oxygen and NO_2 to form the respective peroxyacyl nitrate. Only the formyl radical, which would result from the reaction with formaldehyde, cannot add oxygen. The reaction products in this case are HO_2 and CO rather than HCO_3 (*23*), and this leads to a loss of peroxyacyl nitrate.

For a wall-conditioned flask, the decline of the PAN mixing ratio with time is very reproducible. Instead of preparing PAN mixtures fresh each time, it would also be possible to calculate the PAN mixing ratio from the expression $m = m_0 \exp(-kt)$, where t is the time after com-

pletion of PAN synthesis. In using this procedure, however, one must tolerate a larger margin of uncertainty because it now involves errors arising from the determination of k in addition to m_0. Accordingly, the range of uncertainty increases with time. For practical purposes, the overall precision is conveniently obtained from linear regression analysis of a semilogarithmic plot of all decay data against time similar to that in Figure 2. For a temperature of 22 °C, the relative error was found to increase from 11% initially to 15% after a period of 8 h. The first value is the standard deviation associated with the intercept of the straight line with the ordinate of the plot, the second value results from the combination of the standard deviations for the slope of the line and the intercept.

It is interesting to note that methyl nitrate is not a product of PAN decomposition under our conditions. The concentration of $MeONO_2$ remained constant with time while that of PAN declined (compare Figure 2). Senum et al. (*18*) have suggested that PAN can undergo homolytic scission to form $MeONO_2$ and CO_2. However, the rate coefficient given for $T = 22$ °C, $k = 7.98 \times 10^{-7}$ s^{-1}, is too small to make the process effective on the time scale explored here.

The origin of methyl nitrate is not completely clear. The only reaction known to produce this compound under our conditions is the combination of methoxyl radicals with NO_2. The reaction sequence involves

$$CH_3 + O_2 \rightarrow CH_3O_2 \quad (5)$$

$$CH_3O_2 + NO_2 \rightarrow CH_3O_2NO_2 \quad (6)$$

$$CH_3O_2NO_2 \rightarrow CH_3O_2 + NO_2 \quad (-6)$$

$$CH_3O_2NO_2 + h\nu \rightarrow CH_3O + NO_3 \quad (7)$$

$$2CH_3O_2 \rightarrow CH_3OH + CH_2O + O_2 \quad (8a)$$

$$2CH_3O_2 \rightarrow 2CH_3O + O_2 \quad (8b)$$

$$CH_3O_2 + CH_3COO_2 \rightarrow CH_3O + CH_3 + CO_2 + O_2 \quad (9)$$

$$CH_3O + O_2 \rightarrow HCHO + O_2 \quad (10)$$

$$CH_3O + NO_2 \rightarrow CH_3ONO_2 \quad (11)$$

These must be added to reactions 1–3 and several others, which convert HO_2 radicals to peroxides. We have calculated $MeONO_2$/PAN product ratios by computer simulations based on this reaction scheme with rate coefficients taken from the compilation of Atkinson et al. (*23*). The absorption cross section for $MeONO_2$ is 3×10^{-19} cm^2 (*24*), and a quantum yield ϕ unity was assumed for reaction 7. The $MeONO_2$/PAN ratios calculated were 0.64%, 0.81%, and 1.04% for NO_2 mixing ratios of 7.7, 10.4, and 14 ppm, respectively. The observed $MeONO_2$/PAN ratios of 9.7%, 7.3%, and 7.6% are higher and essentially independent of the NO_2 mixing ratio. This suggests the occurrence of at least one other reaction producing methyl nitrate. The calculated low yield is largely due to the fact that the intermediate formation of methylperoxy nitrate keeps the concentration of NO_2 low during the photolysis period, so that the competition between reactions 10 and 11 favors the former rather than the latter. We have therefore looked at the possibility that the hypothetical reaction

$$CH_3O + CH_3O_2NO_2 \rightarrow CH_3ONO_2 + CH_3O_2 \quad (12)$$

might contribute to the formation of $MeONO_2$. The calculations show, however, that an unrealistically high value for the rate coefficient of reaction 11, namely $k_{11} \approx 4 \times 10^{-11}$ cm^3/(molecule s) would be needed to bring the $MeONO_2$/PAN ratio up to the observed levels. This is unlikely for a typical displacement reaction such as reaction 12. Although we have speculated on a number of other potential processes for the formation of methyl nitrate, none were compatible with the observations. Accordingly, we are unable to identify the true source of excess $MeONO_2$ production.

Finally we discuss PAN generation in the continuous-flow reactor. Grosjean et al. (*12*) have previously described a portable continuous PAN generator based on the reaction of chlorine atoms with acetaldehyde for the production of acetyl radicals. Chlorine atoms were produced by the photodissociation of molecular chlorine with black lamps. Chlorine, acetaldehyde, and nitrogen dioxide were introduced into an airstream from thermostated permeation tubes. The PAN output rate was reported as 64 ± 0.9 ppb. The PAN generator described here is simpler to construct as it does not require an oven with temperature control for keeping permeation rates stable. The relatively high PAN mixing ratio of ~10 ppm obtained with the present procedure is not necessarily a bonus in view of the limited range of linearity of the ECD. Although it is clearly possible to reduce the NO_2 content in the air supply, experience shows that such mixtures, when kept in steel cylinders, are reasonably stable for extended periods of time only for NO_2 mixing ratios of ~1 ppm or greater. However, the PAN mixing ratio generated on-stream may be further scaled down by dilution with clean air. Alternatively, microsyringes may be used for the transfer of samples. We have used the second technique for on-site calibrations and have never experienced any difficulties.

Registry No. PAN, 2278-22-0; MeC(O)Me, 67-64-1; $MeONO_2$, 598-58-3; NO_2, 10102-44-0.

Literature Cited

(1) Singh, H. B. *Environ. Sci. Technol.* **1987**, *21*, 320–327.
(2) Stephens, E. R. *Adv. Environ. Sci.* **1969**, *1*, 119–146.
(3) Nielsen, T.; Samuelson, U.; Grennfeld, P.; Thomsen, E. L. *Nature* **1981**, *293*, 553–555.
(4) Heuss, J. M.; Glasson, W. A. *Environ. Sci. Technol.* **1968**, *2*, 1109–1116.
(5) Taylor, O. C. *J. Air. Pollut. Control Assoc.* **1969**, *19*, 347–351.
(6) Crutzen, P. J. *Annu. Rev. Earth Planet. Sci.* **1979**, *7*, 443–472.
(7) Nielsen, T.; Hansen, A. M.; Thomsen, E. L. *Atmos. Environ.* **1982**, *16*, 2447–2450.
(8) Gaffney, J. S.; Fajer, R.; Senum, G. I. *Atmos. Environ.* **1984**, *18*, 215–218.
(9) Holdren, M. W.; Spicer, C. W. *Environ. Sci. Technol.* **1984**, *18*, 113–116.
(10) Meyrahn, H.; Helas, G.; Warneck, P. *J. Atmos. Chem.* **1987**, *5*, 405–415.
(11) Gay, B. W.; Noonan, R. C.; Bufalini, J. J.; Hanst, P. L. *Environ. Sci. Technol.* **1976**, *10*, 82–85.
(12) Grosjean, D.; Fung, K.; Collins, J.; Harrison, J.; Breitung, E. *Anal. Chem.* **1984**, *56*, 569–573.
(13) Hatchard, C. G.; Parker, C. A. *Proc. R. Soc. London* **1956**, *A235*, 518–536.
(14) Deister, U.; Warneck, P. *J. Phys. Chem.* **1990**, *94*, 2191–2198.
(15) Schurath, U.; Kortmann, U.; Glavas, S. *Physico-Chemical Behaviour of Atmospheric Pollutants*, Proceedings of the Third European Symposium, Varese, Italy, Reidel: Dordrecht, The Netherlands, 1984; pp 27–43.
(16) Cox, R. A.; Roffey, M. J. *Environ. Sci. Technol.* **1977**, *11*, 900–906.
(17) Hendry, D. C.; Kenley, R. A. *J. Am. Chem. Soc.* **1977**, *99*, 3198–3199.
(18) Senum, G. I.; Fajer, R.; Gaffney, J. S. *J. Phys. Chem.* **1986**, *90*, 152–156.
(19) Meyrahn, H.; Pauly, J.; Schneider, W.; Warneck, P. *J. Atmos. Chem.* **1986**, *4*, 277–291.

(20) Weast, R. C., Ed. *CRC Handbook of Chemistry and Physics*, 61st ed.; The Chemical Rubber Co.: Cleveland, OH 1980.
(21) Kirchner, W. Dark Reactions of Nitrogen Oxides in a Smog Chamber, Measurements and Model Calculations. Master's Thesis, University of Bonn, 1986.
(22) Zerbach, T. Organic Nitrates in the Atmosphere. Doctoral Thesis, University of Mainz, 1990.
(23) Atkinson, R.; Baulch, D. L.; Cox, R. A.; Hampson, R. F.; Kerr, J. A.; Troe, J. J. *J. Phys. Chem. Ref. Data* **1989**, *18*, 881–1097.
(24) Roberts, J. M. *Atmos. Environ.* **1990**, *24A*, 243–287.

Received for review March 6, 1991. Revised manuscript received July 19, 1991. Accepted July 22, 1991. The present study has received support from the Germany Federal Ministry of Research and Technology.

Chromium(III) Oxidation by δ-MnO_2. 1. Characterization

Scott E. Fendorf* and Robert J. Zasoski

Department of Land, Air, and Water Resources, University of California, Davis, California 95616

■ The oxidation of Cr(III) by a common naturally occurring form of manganese oxide, δ-MnO_2, was characterized over a range of Cr(III) concentrations and pH values. Cr(III) oxidation was limited as pH and Cr(III) concentrations increased. Reaction products, Mn(II) and Cr(VI), did not limit Cr(III) oxidation. Initial Cr(III) oxidation rates were very rapid at pH = 5, but were subsequently followed by a dramatic rate decline. Thermodynamic calculations using solution species indicated the reaction should proceed under conditions where the reaction had terminated. A surface alteration induced by Cr(III) at pH > 3.5 appears to prohibit the extent of oxidation. Various mechanisms may account for the electrophoretic mobility and oxidation reactions; however, surface precipitation of chromium hydroxide seems to be the most plausible explanation based on our results. Chromium oxidation was dependent on Cr(III) concentration, pH, initial surface area, and ionic strength.

Introduction

The environment is sensitive to heavy metals due to their longevity and toxicity. Chromium is a heavy metal that has many uses in the metallurgic, refractory, chemical, and tannery industries. Chromium oxidation states range from −2 to +6, but only the +3 and +6 states are stable under most surficial conditions. Cr(III) is considered to be less toxic than Cr(VI), and levels greater than 1.7 ppm Cr(VI) in effluent water exceed regulatory limits (*1*). Although Cr(III) compounds have no established mammalian toxicity and pose a low health risk, Cr(VI) compounds are more toxic. Cr(VI) is a carcinogen, an irritant, and a corrosive, which can be absorbed by ingestion, through the skin, and by inhalation (*2*). Cr(VI) is mobile in most soil and water systems, while Cr(III) is rather immobile due to its limited solubility, sorption by negatively charged surfaces prevalent in soils and sediments, and complexation by insoluble organic material. Thus, disposal of Cr(III) is considered to be less problematic than Cr(VI); however, the hazard of Cr(III) is tantamount to Cr(VI) if oxidation occurs.

Cr(VI) can be reduced in many soil systems by reaction with organic matter, Fe(II), and sulfide compounds. Although a variety of compounds are capable of reducing Cr(VI), the only common naturally occurring oxidizing agents of Cr(III) include molecular oxygen and manganese oxides (*3*). Small amounts of Cr are oxidized by O_2 at pH values greater than 9, but these conditions are uncommon in soil or water environments. However, Cr(III) oxidation in soils was only hypothesized, and first studies (*4*) indicated Cr(III) was not oxidized in soils. Bartlett and James (*5*) demonstrated that Cr(III) could be oxidized using fresh rather than dried aged soil samples. It appears that manganese oxides are the principle oxidizing agents for Cr(III) in soil systems.

Bartlett and James (*5*) and Amacher and Baker (*6*) listed possible half-reactions for the oxidation–reduction reaction involving Cr(III) and manganese oxides. Using half-reactions which were assumed to be representative of many environmental conditions, Amacher and Baker (*6*) proposed an overall reaction involving MnO_2 and Cr^{3+}, forming $HCrO_4^-$:

$$Cr^{3+} + 1.5\delta\text{-}MnO_2 + H_2O = HCrO_4^- + 1.5Mn^{2+} + H^+ \quad (1)$$

The forward reaction is not thermodynamically favorable under standard conditions [$\Delta G° = 2.48$ kJ mol^{-1} using thermodynamic values from Garrels and Christ (*7*)]. However, for conditions reflective of surface environmental conditions, ΔG for the reaction can be negative.

Amacher and Baker (*6*) examined surface effects on rates of Cr(III) oxidation by δ-MnO_2. At pH ≥ 5.5, rapid initial Cr(III) oxidation rates were followed by decreasing rates and cessation of the reaction prior to complete utilization of either Cr(III) or MnO_2. They suggested that the decreased rates could only occur if the available reactive surface was "used up" as the reaction proceeded. Increasing MnO_2 levels retarded the onset of the reaction rate decrease, thus enhancing the extent of Cr(III) oxidation. Amacher and Baker (*6*) postulated that competition for adsorption sites between Cr(III) and Mn(II) limited Cr(III) oxidation. These authors assumed a weak association between Cr(III) and δ-MnO_2, followed by a rapid oxidation and subsequent repulsion of negatively charged Cr(VI). However, δ-MnO_2 has a demonstrated strong affinity for various cationic metals (*8–12*). Solution data indicated 1.5Mn(II) was released for each Cr(VI) formed, which supported the proposed stoichiometry. Therefore, since all the Mn(II) expected to form was found in solution, it does not appear likely that adsorption of Mn(II) inhibited Cr(III) oxidation.

Effects of pH on Cr(III) oxidation are unresolved. The rate of Cr(III) oxidation by δ-MnO_2 increased with pH until pH = 5.5; thereafter, the rates were not altered by increased pH (*6*). In contrast, equilibrated soil systems have shown that the extent of Cr(III) oxidation decreased with increased pH (*5*). The rate of Cr(III) oxidation by β-MnO_2 (pyrolusite) was found to increase with decreasing pH (*3*). Eary and Rai (*3*) developed a model for the rate of Cr(III) oxidation by pyrolusite, which was based on Cr(VI) levels as the limiting parameter in the oxidation process. Pyrolusite would have a net positively charged surface throughout the pH range of their study. Eary and

* Present address: Dept. of Plant and Soil Sciences, University of Delaware, Newark, DE 19717-1303.

0013-936X/92/0926-0079$03.00/0